ADVANCES IN ATMOSPHERIC SCIENCES, VOL. 29, NO. 4, 2012, 795–809

Uptake and Storage of Anthropogenic CO_2 in the Pacific Ocean Estimated Using Two Modeling Approaches

LI Yangchun (李阳春) and XU Yongfu* (徐永福)

State Key Laboratory of Atmospheric Boundary Layer Physics and Atmospheric Chemistry,

Institute of Atmospheric Physics, Chinese Academy of Sciences, Beijing 100029

(Received 13 September 2011; revised 30 December 2011)

ABSTRACT

A basin-wide ocean general circulation model (OGCM) of the Pacific Ocean is employed to estimate the uptake and storage of anthropogenic CO_2 using two different simulation approaches. The simulation (named BIO) makes use of a carbon model with biological processes and full thermodynamic equations to calculate surface water partial pressure of CO_2, whereas the other simulation (named PTB) makes use of a perturbation approach to calculate surface water partial pressure of anthropogenic CO_2. The results from the two simulations agree well with the estimates based on observation data in most important aspects of the vertical distribution as well as the total inventory of anthropogenic carbon. The storage of anthropogenic carbon from BIO is closer to the observation-based estimate than that from PTB. The Revelle factor in 1994 obtained in BIO is generally larger than that obtained in PTB in the whole Pacific, except for the subtropical South Pacific. This, to large extent, leads to the difference in the surface anthropogenic CO_2 concentration between the two runs. The relative difference in the annual uptake between the two runs is almost constant during the integration processes after 1850. This is probably not caused by dissolved inorganic carbon (DIC), but rather by a factor independent of time. In both runs, the rate of change in anthropogenic CO_2 fluxes with time is consistent with the rate of change in the growth rate of atmospheric partial pressure of CO_2.

Key words: anthropogenic CO_2, biological process, perturbation approach, Revelle factor, flux

Citation: Li, Y. C., and Y. F. Xu, 2012: Uptake and storage of anthropogenic CO_2 in the Pacific Ocean estimated using two modeling approaches. *Adv. Atmos. Sci.,* **29**(4), 795–809, doi: 10.1007/s00376-012-1170-4.

1. Introduction

The ocean has an important role in the modulation of the concentration of atmospheric carbon dioxide (CO_2). Many models and observations estimate that ∼40% of the total anthropogenic CO_2 released by human activities has been absorbed by the global ocean over the past 200 years. However, the uncertainty of the air-sea CO_2 flux is still very large (Solomon et al., 2007). To accurately project the oceanic uptake of anthropogenic CO_2 under the future global climate change, the uncertainty in estimations of present and future levels of ocean carbon sink must be reduced.

Since the distribution of global ocean carbon sinks and sources was described with the observations by Keeling (1968), many estimates of air-sea CO_2 fluxes have been made with the increased amount of observations (Takahashi et al., 2002, 2009; Sweeney et al., 2007; Gruber et al., 2009). In addition to these observations, there are two categories of ocean carbon models to estimate the air-sea CO_2 flux, including the inverse models with the observed data and the ocean general circulation models (Gloor et al., 2003; Mikaloff et al., 2006; Sweeney et al., 2007; Gruber et al., 2009), and the forward dynamics carbon models. For the forward models, because of different physical models and simulation procedures, large differences occur among the simulation results. Orr et al. (2001) compared the uptake of anthropogenic CO_2 in four three-dimensional (3D) ocean models, which were part of the first phase of the Ocean Carbon-Cycle Model Intercomparison Project (OCMIP), in which

*Corresponding author: XU Yongfu, xyf@mail.iap.ac.cn

the abiotic, biotic, or perturbation approaches were used, respectively, and found that the simulated uptake agreed among them at a rate of ±19%. Matsumoto et al. (2004) also indicated that only ∼25% of 19 carbon-cycle models were consistent with the data-based metrics from the distributions and inventories of trichlorofluoromethane, known as CFC-11 (or the DuPont trade name Freon-11), and new radiocarbon data. Those studies showed that the differences among the models were caused by different parameterizations of the physical fields. In addition, we also need to quantify the difference induced by the different simulation methods for carbon cycle to determine the main cause of these differences.

Primarily two types of forward ocean carbon-cycle models directly simulate anthropogenic CO_2 in the ocean. One adopts an ocean carbon cycle model with biological processes to consider the effect of ocean biota on the oceanic uptake of atmospheric CO_2, and the other uses the perturbation approach proposed by Sarmiento et al. (1992), which is based on the knowledge that the effect of the change of ocean biota on the uptake of anthropogenic CO_2 is minor (Murnane et al., 1999).

Biological processes are generally described in different ways in the different ocean carbon-cycle models. In the second phase of the OCMIP (OCMIP-2), the biogeochemical model based on the phosphate cycle was adopted in many ocean carbon-cycle models (Najjar et al., 2007), and it was applied in the climate system models in the Coupled Carbon Cycle Climate Model Intercomparison Project (C^4MIP) (Friedlingstein et al., 2006). The perturbation approach provides a simple and convenient way of estimating the oceanic uptake of anthropogenic CO_2 with the application of the uniform alkalinity and salinity in the ocean. The results based on this approach are comparable to the observation-based results (Sarmiento et al., 1992; Siegenthaler and Joos, 1992; Xu et al., 2000; Müller et al., 2006; Xu and Li, 2009). Compared with the carbon-cycle models that consider biological processes, the perturbation approach can significantly reduce the computational time, so it is more suitable to application in a high-resolution model (Lachkar et al., 2009). In this study we aim to investigate the difference between the results from these two popular approaches in detail and to quantify their differences to reduce uncertainty in estimating air-sea carbon flux.

To perform in-depth studies of the ocean carbon cycle, many researchers have given more attention to particular oceanic regions when studying the role of the ocean physics and biogeochemistry in the uptake of anthropogenic carbon. Because the Pacific Ocean has the largest area and the strongest interannual variability in the climate system (ENSO) occurs there, many researches have been made on the carbon cycle in the Pacific Ocean. Based on observations, Takahashi et al. (2009) estimated that the tropical Pacific accounts for 70% of the outgassing of CO_2 in the global tropical ocean (14°S–14°N). Because of ENSO events, 70% of the interannual variability of global ocean carbon budget mainly occurs in the equatorial Pacific (Le Quéré et al., 2000). The tropical Pacific Ocean is also an important absorbing region for anthropogenic CO_2, and it dominates the uptake of anthropogenic CO_2 in the tropics (Orr et al., 2001). In addition to the tropical Pacific, the North Pacific Ocean is also an important sink of anthropogenic CO_2. Observation data has been used to estimate the storage of anthropogenic CO_2 in the North Pacific (Sabine et al., 2002). An annual mean increase of 0.43 mol m^{-2} yr^{-1} in anthropogenic CO_2 inventory along 30°N in the North Pacific between 1994 and 2004 has also been obtained based on the observations (Sabine et al., 2008). The uptake of anthropogenic CO_2 in the North Pacific Ocean was estimated by the global model (Rodgers et al., 2008) and by the North Pacific model with the perturbation method and with different isopycnal diffusion coefficients (Xu et al., 2000). The results of these model simulations show a full seasonal cycle of the uptake of anthropogenic CO_2 that cannot be well resolved with the observations. The maximum uptake of anthropogenic CO_2 in the North Pacific occurs in winter (Rodgers et al., 2008). The storage estimated by the model of Xu et al. (2000) is larger than the observation-based storage estimates (Sabine et al., 2002). The smaller the adopted isopycnal diffusivity in the Gent-McWilliams tracer-mixing scheme (Gent and McWilliams, 1990; Gent et al., 1995), the closer the simulation to the observations (Xu et al., 2000). In 2009, Xu and Li (2009) re-estimated the storage of anthropogenic carbon in the Pacific Ocean using a global general circulation model (L30T63) developed by the Institute of Atmospheric Physics; the estimate resulting from this model is also less than the observation-based estimate.

The purposes of this study are to use a Pacific basin model for the investigation of the uptake, storage, and distribution of anthropogenic CO_2 in the Pacific Ocean using two different approaches: the PTB simulation and the BIO model simulation, and to determine the causes of the discrepancies in the simulated results of these two approaches. In addition, we also evaluate the ocean carbon-cycle general circulation model of the Pacific Ocean by comparing its results with those derived from the observations. The observed data regarding dissolved inorganic carbon (DIC) and anthropogenic carbon are obtained

from the Carbon Dioxide Information Analysis Center (CDIAC, http://cdiac.ornl.gov), presented by the Global Ocean Data Analysis Project (GLODAP; Key et al., 2004). For that database, the datasets were mainly collected between 1985 and 1999, including some data from the Geochemical Ocean Sections Program (GEOSECS) during the 1970s.

2. Model and experiment descriptions

2.1 *The Pacific Ocean model*

The basin-wide ocean general circulation model (OGCM) of the Pacific Ocean is configured from a 3D global OGCM called LICOM (Liu et al., 2004; Yuan and Liu, 2009). With the basic frame of LICOM (e.g., the primary equation, free surface, η-vertical coordinate, the Arakawa B-grid scheme), the model domain is the entire Pacific Ocean (latitude 75°S–65°N and longitude 98°–291°E) with the horizontal resolution 1.0°×1.0°. This model includes 26 unequal vertical levels with the maximum depth of 5500 m, and the thickness of the upper 10 levels is 100 m. To obtain a reasonable Antarctic circulation that is relatively homogeneous in the zonal direction, we treat the western and eastern boundary conditions as cyclic ones. To do this, we artificially set the both westernmost and easternmost two columns of grids as the solid wall from 10°N to 50°S, and as the water region from 50°S to the Antarctic, respectively. Correspondingly, the Drake Passage is widened. The GM mixing parameterization of tracers (Gent and McWilliams, 1990; Gent et al., 1995) is adopted in this basin model with the same isopycnal and thickness diffusion coefficients (1.0×10^3 m^2 s^{-1}).

The OGCM is forced at the surface by climatology boundary conditions of thermal fluxes, salinity and wind stress. Sea-surface temperature (SST) and sea-surface salinity (SSS) data are obtained from WOA98 (http://www.nodc.noaa.gov/), and other forcing data are obtained from MPI-OMIP climatological monthly mean data (Roeske, 2001). Because of the absence of a sea-ice model, to produce a realistic physical field for the tracer transport, temperature and salinity are restored to climatological data (WOA98) below the first layer at higher latitudes in the both hemispheres to specify the water features. Within 20° of the two boundaries, the restoration time scales of 1 year and 6 months are used for the northern boundary and southern boundary, respectively. This model is able to accurately reproduce the main physical field characteristics, including the distribution of water masses, the circulation and the heat transport, whereas the Antarctic Circumpolar Current is overestimated with the maximum of 180 Sv (1 Sv=10^6 m^3 s^{-1}) because of the widening of the Drake Passage (Xu et al., 2006). Prior to this study, the model was assessed using the simulated distribution and inventory of CFC-11 (CCl_3F). Results show that the simulated distribution of CFC-11 agrees well with observation data, although there is some deficiency of the penetration depth in the subtropical North Pacific.

2.2 *Ocean carbon model*

Two different carbon approaches are used in this work to estimate the distribution and storage of anthropogenic CO_2 in the Pacific Ocean, including the perturbation approach and the carbon cycle model with biological processes, which are described in the following subsections.

2.2.1 *Perturbation approach*

Based on the perturbation approach proposed by Samiento et al. (1992), we solved an advection-diffusion equation of anthropogenic CO_2 in the ocean. Anthropogenic CO_2 absorbed by the ocean is transported and restored in the ocean interior as passive tracer. The surface layer exchanges anthropogenic CO_2 with the atmosphere, whereas the atmosphere is treated as a well-mixed box. The concentration of anthropogenic carbon in the both ocean and atmosphere is defined as zero at the beginning of the simulation (time 0) that is considered to represent 1800. The flux of air-sea anthropogenic carbon can be written as follows:

$$F = K_g \left(\delta p_{\mathrm{CO_{2a}}} - \delta p_{\mathrm{CO_{2o}}}\right) , \tag{1}$$

where K_g is the exchange coefficient of CO_2 at the air-sea interface, which is the product of the transfer velocity and solubility of CO_2 in the surface water. Transfer velocity is a function of wind speed and seawater temperature, which is calculated from Waninkhof (1992). The data for wind speed are obtained from Esbensen and Kushnir (1981). $\delta p_{\mathrm{CO_{2a}}}$ and $\delta p_{\mathrm{CO_{2o}}}$ indicate the perturbations of atmospheric partial pressure of CO_2 ($p_{\mathrm{CO_{2a}}}$) and ocean surface partial pressure of CO_2 ($p_{\mathrm{CO_{2o}}}$) at time t, relative to their values at time 0. The equation proposed by Sarmiento et al. (1992) relating $\delta p_{\mathrm{CO_{2o}}}$ to δDIC (total inorganic anthropogenic carbon in the ocean) is used, assuming a constant salinity of 35 psu (g kg^{-1}) and constant alkalinity of 2300 μmol kg^{-1}:

$$\begin{aligned} \delta p_{\mathrm{CO_{2o}}} &= \frac{z_0 \delta\mathrm{DIC}}{1 - z_1 \delta\mathrm{DIC}} \\ z_0 &= 1.7561 - 0.031618T + 0.0004444T^2 \\ z_1 &= 0.004096 - 7.70806\times10^{-5}\times T + \\ &\quad 6.10\times10^{-7}\times T^2 , \end{aligned} \tag{2}$$

where T is the sea surface temperature in °C.

2.2.2 *Biogeochemistry model*

The biogeochemistry model basically consists of inorganic carbon processes and biological processes. The transport of DIC in the biogeochemistry model is formally quite similar to that in the anthropogenic carbon model except that there is an additional term due to biological processes. The exchange flux of CO_2 at the air-sea interface is the same as that of anthropogenic CO_2 in the absence of δ, which is written as follows:

$$F = K_g \left(p_{\mathrm{CO_{2a}}} - p_{\mathrm{CO_{2o}}} \right) . \tag{3}$$

Unlike anthropogenic CO_2, the partial pressure of CO_2 is not a perturbed value but a realistic value. $p_{\mathrm{CO_{2o}}}$ is computed in terms of the iteration method using thermodynamic equations interrelating the carbonate system parameters: the simulated temperature, salinity, total alkalinity (TA), and DIC (Peng, 1987; Xu, 1992).

The biological processes are mainly concerned with four geochemical tracers: DIC, TA, phosphate, and dissolved organic carbon (DOC). The new production exported out of the euphotic zone is the function of the difference between the simulated and observed phosphate (Najjar et al., 1992, 2007):

$$J_{\mathrm{np}} = \sigma \times \frac{1}{\tau} \left(\left[PO_4^{3-} \right]_{\mathrm{model}} - \left[PO_4^{3-} \right]_{\mathrm{obs}} \right) , \tag{4}$$

where the time scale τ is 100 days and the parameter σ is 1 (or 0) when modeled phosphate is larger (or smaller) than observed phosphate levels. A depth of 100 m for the euphotic zone is used in the biogeochemical model. New production is evenly divided into two parts: particle organic matter (POM) and dissolved organic matter (DOM); both are remineralized below the euphotic zone. The vertical profiles of the vertical flux of POM proposed by Yamanaka and Tajika (1996) and of DOM by Anderson and Sarmiento (1995) are used in the model, respectively. For the conservation of global TA, a diagnostic variable calcium carbonate is included in the model, which is calculated in terms of the difference between the global vertical profiles of observed and simulated TA (Murnane et al., 1999). All other process variables relating to carbon and biological processes are calculated with new production and the Redfield ratio (C:N:P=120:16:1), directly and indirectly.

2.3 *Numerical experiments*

After 1600 years of integration of OGCM under the climatological forcing data, the physical fields reached an equilibrated status in which the model domain mean temperature change is <0.005°C per century at each of the 26 vertical levels. The biogeochemistry model is incorporated into the OGCM, and then the carbon-cycle circulation model is run from the equilibrated physical status and the observed profiles of DIC, TA, and phosphate from WOA-CDIAC (http://cdiac.ornl.gov) under the climatological physical forcing data and the atmospheric CO_2 of 278 ppmv that is defined as the preindustrial value in 1800. The observed monthly climatology phosphate is used in the model to calculate the export production. The initial concentration of DOC is 4.2 μmol kg^{-1}. After the 5000-year integration, the flux of air-sea CO_2 is small enough to be ignored, and this status is treated as the preindustrial result. Based on the preindustrial result, the model is integrated from 1800 to 2000 under the realistic atmospheric CO_2 concentration from Enting et al. (1994) and CDIAC (http://cdiac.ornl.gov). This experiment is called as BIO. With the same physical forcing and atmospheric CO_2 data the perturbation simulation is conducted for 200 years from the equilibrated physical status at the year 6600 obtained in BIO, which is called PTB. The initial perturbated DIC in PTB is zero, defined as the status in 1800, and the atmospheric CO_2 forcing data is the realistic atmospheric CO_2 concentration between 1800 and 2000 minus the preindustrial value of 278 ppmv.

3. Results and discussion

The anthropogenic CO_2 (or anthropogenic DIC, anDIC) in the ocean obtained from the two runs is called as excess carbon (hereafter, exDIC) in BIO and perturbed inorganic carbon (ptDIC or δDIC) in PTB, respectively. Excess carbon is derived from the difference between the DIC concentrations at time t and at time 0 (that is the preindustrial equilibrium status, for which the DIC concentration is also called natural DIC).

The modeled and observed DIC in the 1990s are shown in Fig. 1. To be consistent with the period of GLODAP, the simulated result is an average over 10 years from 1990 to 1999. If there is no specific indication in the following text, the simulated results all denote the annual average of this period. The concentrations of surface DIC are affected by SST and the upper layer currents. The distribution of DIC shows a meridional gradient, and the simulation is quantitatively consistent with the observations. In the tropics, the large concentration occurs in the eastern equatorial Pacific, with a maximum value >2010 μmol kg^{-1}, where the upwelling is strong with a maximal velocity of 3×10^{-5} m s^{-1} (Xu et al., 2006) and can transport high-DIC water from the subsurface layer to the surface. The DIC concentration in the warm pool is ∼100 μmol kg^{-1} lower than that in the cold tongue region. In the Southern Ocean the contours of DIC concentrations are generally parallel to the latitude because

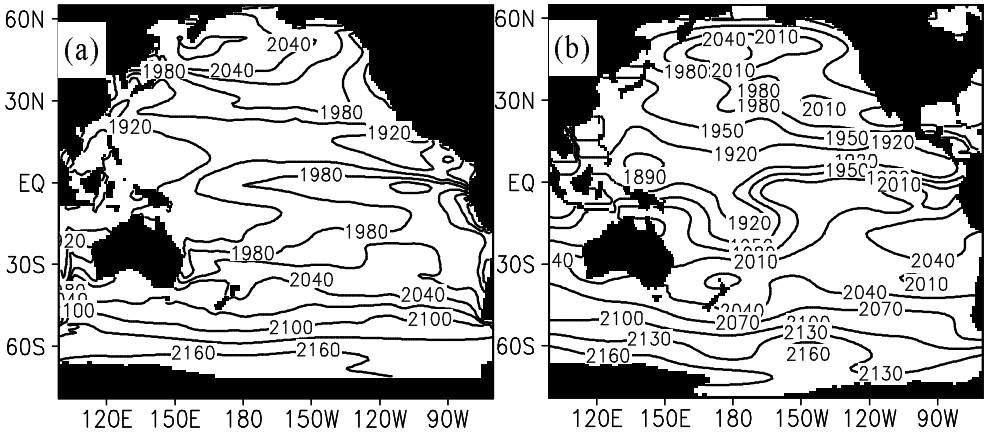

Fig. 1. Distribution of DIC concentrations averaged from 1990 to 1999 (μmol kg^{-1}): (a) simulation, (b) observation. Contour intervals are 30 μmol kg^{-1}.

of the transports of ACC (the Antarctic Circumpolar Current), with the maximum concentration of >2160 μmol kg^{-1} occurring south of 60°S. In the Northern Hemisphere and the southern subtropical region there are obvious zonal gradients, which are affected by the boundary currents. The main differences between the simulation and the observations occur in the high-latitude North Pacific and the equatorial Pacific, where the simulated results are generally larger than the observed value. This result is probably induced by the deficiency of description of complicated currents, especially the equatorial currents in the tropical Pacific which depend on high meridional resolution.

3.1 *Distributions of the modeled sea surface anDIC*

The surface concentration of anthropogenic CO_2 is associated with the strength of local uptake and transport. Certainly, the longer the waters are exposed to the atmosphere, the more anthropogenic CO_2 can be taken up from the atmosphere. Indeed, low anDIC concentrations can be seen in the Southern Ocean (south of 60°S) (Fig. 2). The strong vertical movement in the Southern Ocean transports the absorbed anthropogenic CO_2 into the deep water quickly. The upwelling in the equatorial region leads to the low anthropogenic CO_2 concentration because the anDIC-poor deep water is brought up to the surface. Because of the northern and southern transports from the wind-driven circulation as well as weak vertical movement, the subtropical region has high concentrations of anthropogenic DIC after its long contact with the atmosphere. The distributions of anthropogenic CO_2 concentrations are mostly similar to each other between the two runs under our simulation conditions because of exactly same circulation fields and SST. However, there are some differences in the distribution pattern of anthropogenic CO_2 in the subtropical Pacific Ocean between the two runs. For example, the maximum anthropogenic CO_2 in the central-eastern region of 20°–30°S obtained in BIO cannot be seen in Fig. 2b. In the comparison of exDIC and δDIC, the exDIC concentrations are 6 μmol kg^{-1} and 10 μmol kg^{-1} higher than the δDIC concentration in the northern and southern subtropical regions, respectively, whereas the exDIC concentration is lower than δDIC in the both equatorial and subpolar regions. This demonstrates that the anthropogenic CO_2 flux and the buffer capacity are probably different between the two runs because the physical fields are exactly the same.

In general, the buffer capacity (Revelle factor) decreases with increasing SST and DIC, whereas the capacity for the waters to take up anthropogenic CO_2 decreases with increasing values of buffer capacity (Sabine et al., 2004). To compare with the result based on the observations from the study of Sabine et al. (2004), the simulated Revelle factors are calculated with annual mean sea surface temperature, salinity, DIC, and TA in 1994 according to Eq. (23) of Xu (1992). As shown in Fig. 3a, the distribution of the Revelle factors obtained with our model is in good agreement with the result from Sabine et al. (2004), with the minimum <9 in the western tropical Pacific and the maximum >15 in the southern subpolar region. Therefore, from the aspect of uptake, the tropics and the Southern Ocean should have the highest and lowest concentrations of anthropogenic CO_2, respectively. This hypothesis is consistent with the results of exDIC in Fig. 2a. The consistency between the distributions of the Revelle factors and DIC indicates that the influence of TA and salinity on pCO_2 is not dominant. Thus, the fact that salinity and TA are set as constants in the perturbation approach is reasonable to a large extent. To examine the possible effect in

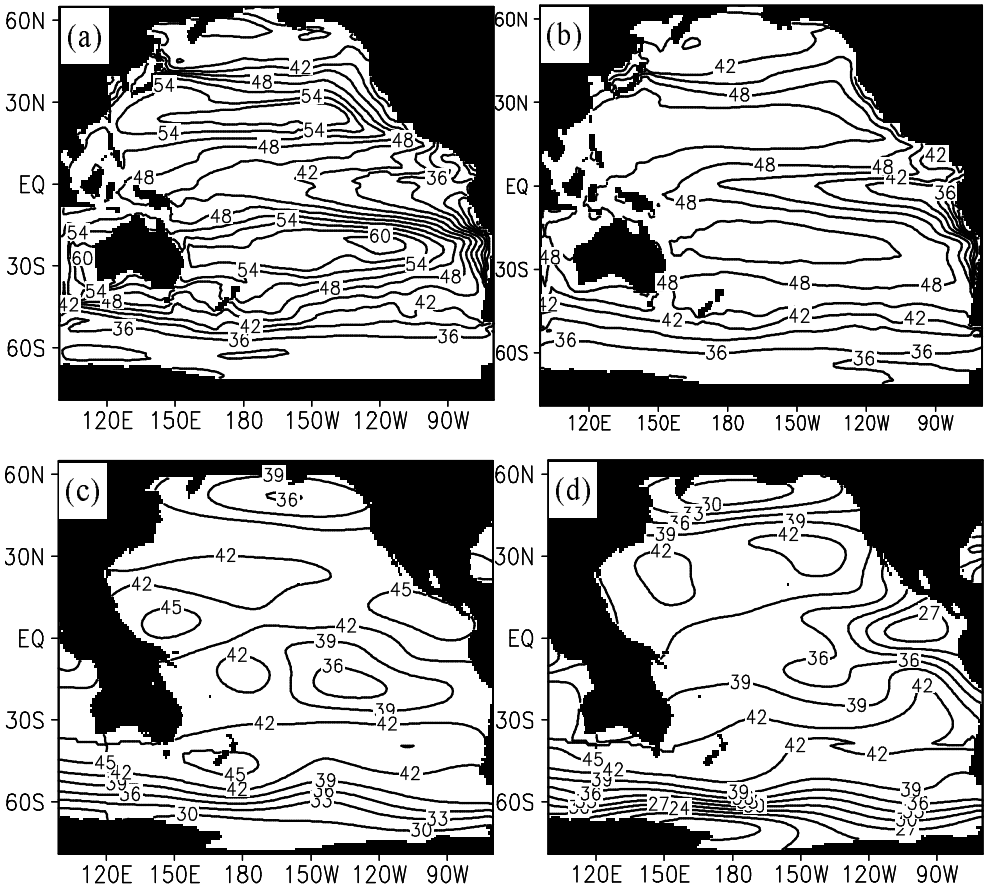

Fig. 2. Surface distribution of anthropogenic CO_2 (μmol kg^{-1}) in the 1990s: (a) BIO, (b) PTB, (c) observation-based (0 m), and (d) observation-based (100 m). Contour intervals are 3 μmol kg^{-1}.

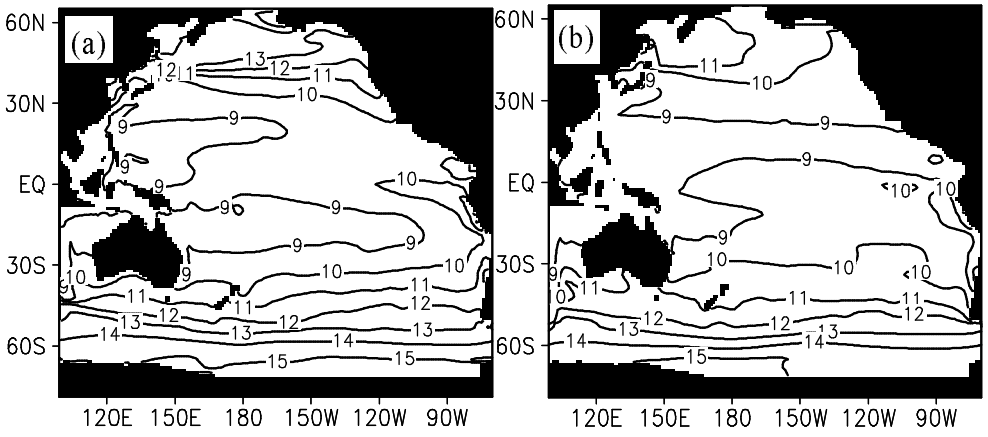

Fig. 3. Distributions of the Revelle factors in 1994: (a) BIO, (b) BIO with constant total alkalinity (2300 μmol kg^{-1}), and salinity (35 psu).

the absence of spatial distributions of TA and salinity, we use the perturbation condition to calculate the Revelle factor, under which TA and salinity are set at 2300 μmol kg^{-1} and 35 psu, respectively, whereas for temperature and DIC the 1994 simulation results are used. The distribution of the Revelle factor in Fig. 3b generally resembles that in Fig. 3a. However, in Fig. 3b lower values appear to be located in some areas in the North Pacific and the equatorial Pacific, and larger values at some areas in the region of 10°–40°S. The difference between the regions in Fig. 3a and b is consistent with the difference in the anthropogenic CO_2 concentrations (Figs. 2a and b), except in the northern subtropical region. The larger the difference in the Revelle factor between these two approaches, the larger the difference in the anDIC concentration. For example, both the differences in anDIC and in the Revelle factor in the high latitudes of the North Pacific are larger than those in the high latitudes of the South Pacific.

Our simulated results of anDIC in the North Pacific are in good agreement with those from the MOM(the Modular Ocean Model)-based circulation model of the North Pacific described in Xu et al. (2000): Maximum values appear to occur at 10°–30°N of the western North Pacific, and there is a west–east gradient in the both subtropical and equatorial regions. Our results are somewhat different from the observation-based estimates by Key et al. (2004), who used the approach of Sabine et al. (2002). In addition to the result that the simulated concentration is generally higher than the observation-based estimate, the meridional gradients of anthropogenic CO_2 obtained from the two simulations are opposite with the observation-based estimates in the tropical and subtropical regions. However, it has not been seen that the simulation in the former researches generated patterns similar to those of the observation-based estimates. In fact, the distribution patterns of simulated anDIC are more consistent with the observation-based results at ∼100 m (Fig. 2d) than with those at the surface, which means that the modeled distributions of sea surface anDIC should be considered representative of realistic distributions of anDIC in the mixed layer, because the observation-based surface anDIC concentration was strongly affected by the choice of observation period (i.e., temporally). Simulated surface anDIC concentrations are higher than the observation-based estimates. This is related to the deficiency of ocean vertical ventilation, which can be improved by the increase of wind stress or vertical diffusion coefficient (Gnanadesikan et al., 2004). This study focused on the difference caused by two different carbon simulation approaches. The influence of the shortness of ocean physics on these two runs is the same. Thus, the effects of physical fields are not discussed further.

3.2 *Vertical distributions of anDIC*

Figure 4 shows a comparison of model-simulated anthropogenic CO_2 with the observation-based estimate of this quantity along the section of 151°W.

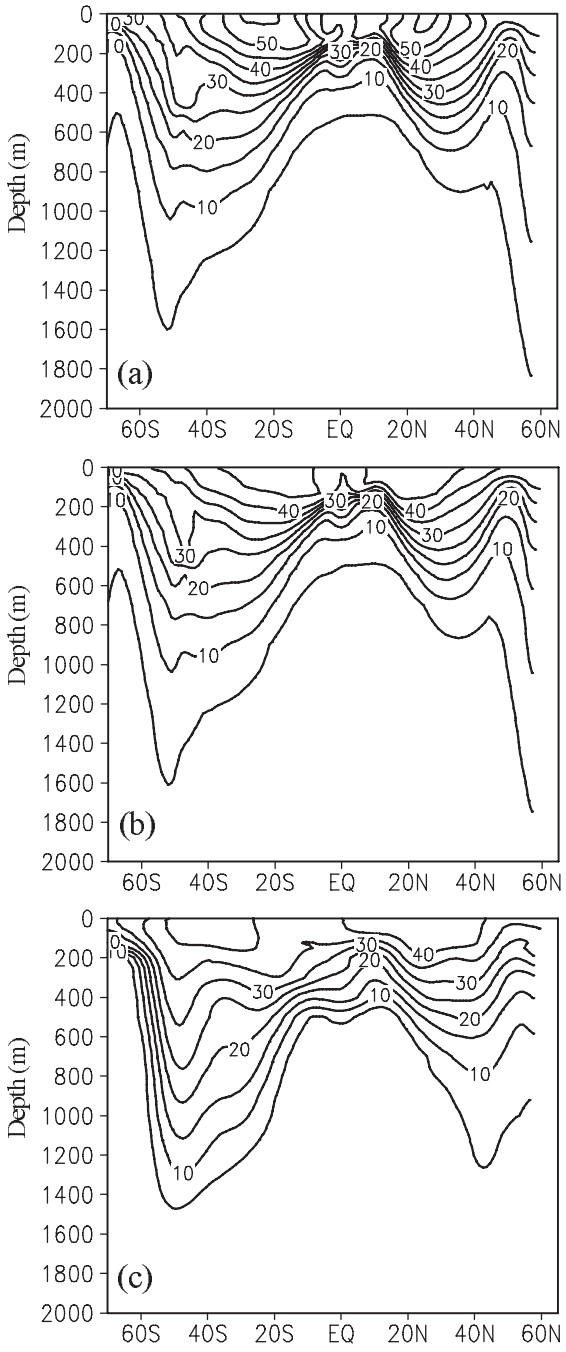

Fig. 4. Anthropogenic CO_2 (μmol kg^{-1}) distribution at 151°W in 1991: (a) BIO, (b) PTB, and (c) observation-based results. Contour intervals are 5 μmol kg^{-1}.

Because the cruise date was January 1991 in the Northern Hemisphere and July 1991 in the Southern Hemisphere, we chose to consider simulated results of the annual mean from 1991. Anthropogenic CO_2 absorbed in the surface water is mainly transported into the ocean interior through the isopycnals. The sinking of surface water caused by convergence in the subtropical region results in water above 200 m depth in this area containing the highest concentration of anthropogenic CO_2. The formation of intermediate water in the both hemispheres and the vertical movement generate the deepest penetrations of anthropogenic CO_2 near 50°S in the South Pacific and near 40°N in the North Pacific, respectively. Except for the region north of 50°N, particularly at 54°–57°N, where the two runs considerably overestimate the observation-based penetration, the observations and simulations shared similar distributions to their isopycnal distributions: a W-shaped structure. The simulated North Pacific intermediate water (NPIW) is weaker than the observation-based NPIW, which lead to the shallower penetration of anthropogenic CO_2 there in the two runs. The penetration of anthropogenic CO_2 near 50°S is overestimated in our models, where the penetration depth of the 5-μmol kg^{-1} contour is 200 m deeper than the observation-based estimate. Orr et al. (2001) evaluated four OGCMs, and pointed out that the three models (i.e., Priceton/GFDL, Hadley and MPI) at a similar section of the Atlantic Ocean overestimated the penetration of anthropogenic CO_2 south of 50°S, whereas the IPSL model considerably underestimated the penetration. The results from our two different carbon models are basically consistent. The main difference is that surface anthropogenic CO_2 in BIO is higher than that in PTB, which is likely due to higher fluxes in BIO. The anthropogenic CO_2 in the upper layer is overestimated in the simulated results, which lead to shallower penetration in the North Pacific; this result demonstrates the need to improve the simulation of thermohaline circulation in our physical model.

Figure 5 displays a comparison of model-simulated anthropogenic CO_2 and observation-based estimates of this quantity at 30°N in January 1994. The observations were collected in January 1994 from the cruise called P02 in WOCE (Key et al., 2004). The simulated results are the average of January 1994. The section at 30°N is a main storage region of passive tracers. Because the section is affected by the circulation system in the North Pacific, there is a large difference in the distribution of passive tracers between the west and east. The distribution of anthropogenic CO_2 is characterized by deep western penetration and shallow eastern penetration. For example, in the 5-μmol kg^{-1} contour, the observation shows that the contour can reach only 500 m on the eastern side, whereas it can reach 1000 m on the western side. The simulated results are basically consistent with the observations. Like the simulated results of bomb ^{14}C at 30°N in the comparison of three models by Orr et al. (2001),

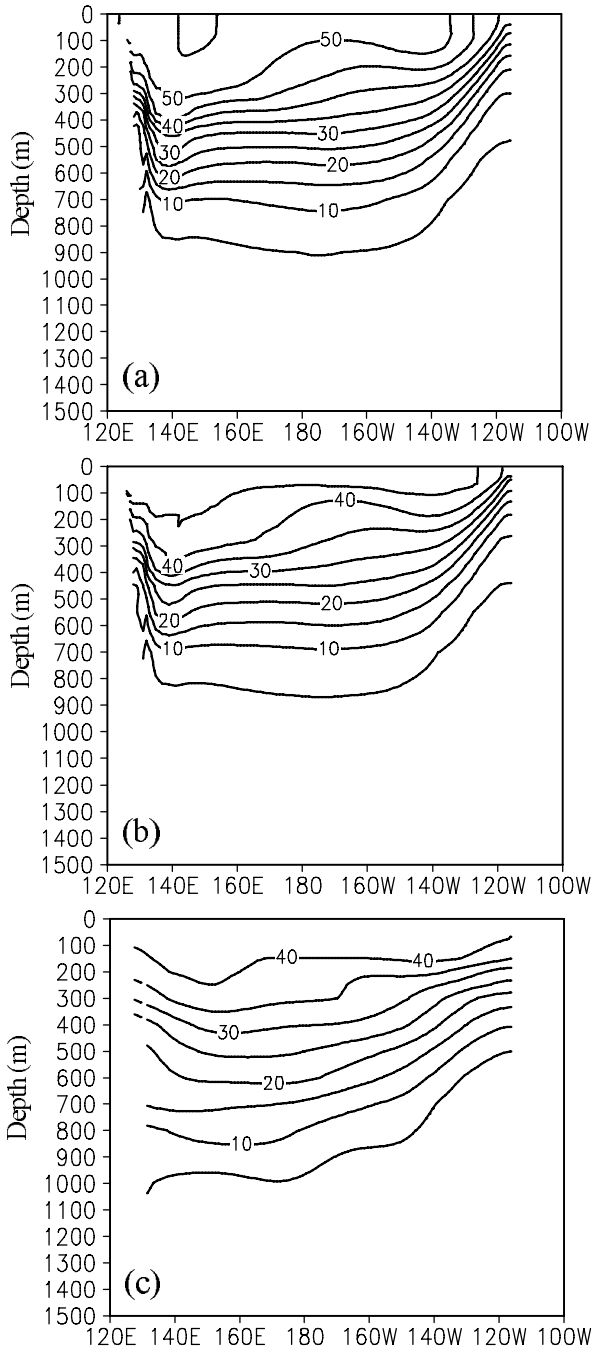

Fig. 5. Anthropogenic CO_2 (μmol kg^{-1}) distribution at 30°N in January 1994: (a) BIO, (b) PTB, and (c) observation-based results. Contour intervals are 5 μmol kg^{-1}.

this further demonstrates that the weak downward and southward transport of NPIW popularly exists in the models. In addition, compared to PTB, the higher surface concentration in BIO did not produce the obviously deeper penetration, which illustrates that the shallow penetration is not mainly generated by the local uptake but rather by the weak vertical transport of the physical fields.

3.3 *Anthropogenic carbon inventory*

Figure 6 shows the simulated anthropogenic carbon inventory in the Pacific Ocean. The high inventory occurs in the subtropical regions, with the maximum inventory >35 mol m^{-2} at ~50°S. In contrast with the Northern Hemisphere, the location of high inventory region in the Southern Hemisphere is at higher latitude, and the value is larger. The inventory in the equatorial region and the higher latitude is lower because the wind-driven circulation removes the anthropogenic carbon absorbed in the local site. The formation of intermediate waters, including NPIW and AAIW, transports the anDIC-rich water downward and equatorward, so that a large amount of anthropogenic CO_2 is stored in the subtropical regions. The simulations match the observation-based estimates of Sabine et al. (2002) in the most regions, with some difference occurring at about 10°N of the western tropical Pacific, where the observation-based estimates show that the inventory is lower on the western side than on the eastern side at the same latitude. Both runs generate an obvious west-to-east gradient of anthropogenic CO_2 in the northern subtropical region, although the location of maximum value in the simulations lies to the west. The main difference in the column inventory between the two runs is produced by the difference of the simulated anDIC concentrations above 400 m. The higher surface anDIC concentration in BIO leads to the higher column inventory.

To compare our results with the estimate of Sabine et al. (2002) in detail, the simulated results in 1994 are used to calculate the zonal mean inventory from 120°E to 70°W (Fig. 6d). Notably, the modeled results include the marginal seas. The maximum inventory of anthropogenic CO_2 in the Pacific Ocean is near 48°S in the observation-based estimate and near 45°S in the simulations. The maximum inventory of 36.0 mol m^{-2} in BIO is greater than that of 34.2 mol m^{-2} in PTB and also greater than the observation-based estimate of ~ 35.4 mol m^{-2}. In the North Pacific there are large differences in the inventory between the two simulations and the observation-based estimate. The two simulations both reveals two high-inventory regions in the whole North Pacific, with the largest one at 25°–30°N and the second largest one at 50°–60°N, whereas the observation-based estimate gives three high-inventory regions, including two regions similar to those of the simulations and one region at 35°–45°N that contains the largest inventory. The reason for the difference in the location of the largest inventory between the simulations and the observation-based estimate is explained by the likelihood that the model-simulated anthropogenic CO_2 surface concentrations are too high in the northern subtropical Pacific and the simulated penetration of anthropogenic CO_2 is shallow at ~40°N, a result associated with the weak NPIW.

The simulated results show that, as of 1994, the Pacific Ocean contained 46.2 Pg C and 43.2 Pg C of anthropogenic carbon according to BIO and PTB, respectively, and that the North Pacific contained 17.0 Pg C and 15.1 Pg C of anthropogenic carbon according to BIO and PTB, respectively. These estimates agreed well with the observation-based estimates of 44.5 Pg C in the Pacific Ocean and 16.5 Pg C north of the equator (Sabine et al., 2002). Different from the estimate by Sabine et al. (2002), our estimate includes the marginal seas in the model domain. Using the MOM-based model, Xu et al. (2000) estimated that, as of 1994, ~1.6–3.4 Pg C of anthropogenic carbon was transported from the North Pacific to the South Pacific, which directly contrasts with our simulated results. Our two runs show an uptake of 16.1 Pg C and 14.4 Pg C by the North Pacific as of 1994 in BIO and PTB, respectively, indicating that ~0.68–0.96 Pg C of anthropogenic carbon was transported into the North Pacific from the South Pacific. Both the uptake and storage from these two runs are smaller than those by Xu et al. (2000). In addition to the differing configurations of MOM and our model, the artificial rigid boundary at 20°S in the Xu et al.'s model probably has some impact on the simulated results.

3.4 *Difference in the anthropogenic carbon flux between the two runs*

From the comparison drawn in the previous section, it can be seen that, under the same vertical transport of anthropogenic CO_2 due to physical processes, the main difference between the two runs is due to the difference caused by accumulation of absorbed anthropogenic CO_2 in the upper layer. The simulated 10-year averaged air-sea exchange fluxes in the 1990s of anthropogenic carbon are shown in Fig. 7. Three main absorbing regions can be seen, where either vertical movement is strong, or convection mixing is frequent, including the equatorial upwelling region, the region of formation of NPIW and the Southern Ocean. The simulated fluxes show that the two runs generate the same basic features; they are consistent with the MOM-simulated result in the North Pacific by Xu et

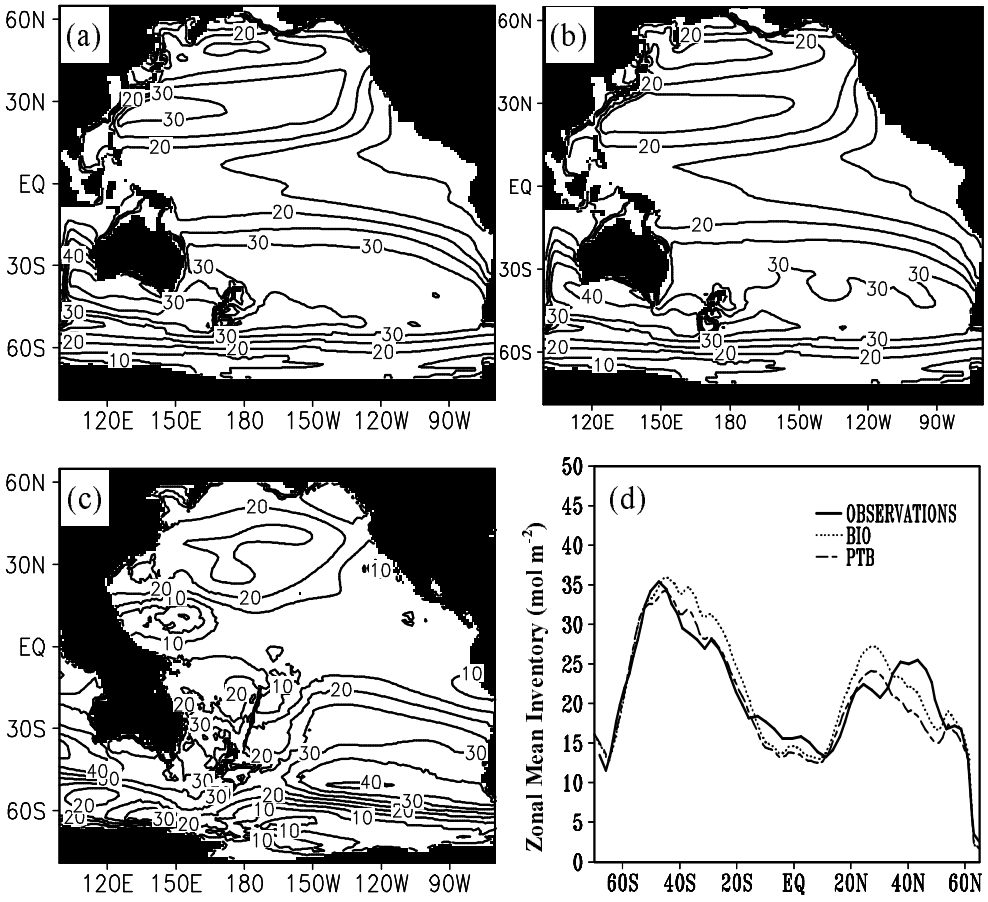

Fig. 6. Distribution of anthropogenic CO_2 column inventory (mol m^{-2}) in the 1990s: (a) BIO, (b) PTB, (c) observation-based results, and (d) zonal mean inventory of anthropogenic CO_2 (mol m^{-2}) in 1994.

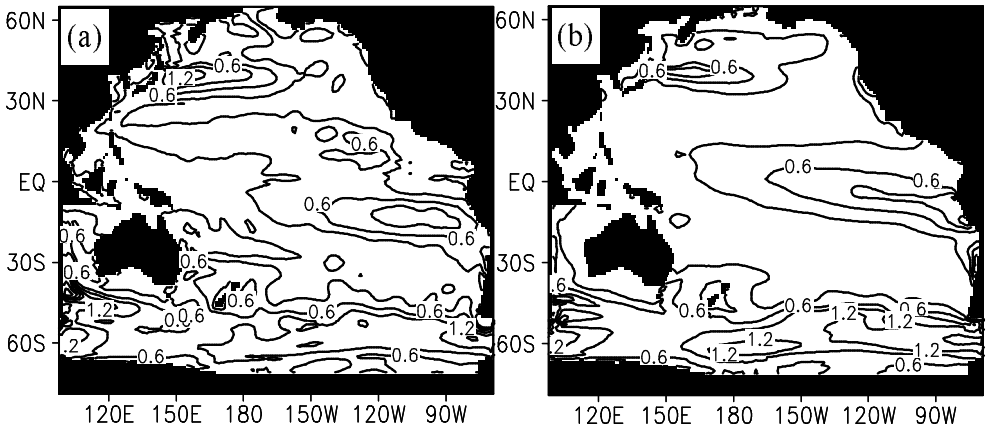

Fig. 7. Distribution of 10-year averaged air-sea exchange fluxes (mol m^{-2} yr^{-1}) of anthropogenic CO_2 in the 1990s: (a) BIO and (b) PTB.

al. (2000). Because of the impacts of TA, the anthropogenic CO_2 flux in BIO is not entirely affected by the upwelling. For example, unlike PTB in which there is only a maximum flux area located south of the equator in the tropics, BIO has two maximum flux areas, one south of the equator and the other at 10°–20°N. In addition, some differences in the absorbing ability in the Southern Ocean are also evident.

To assess the simulated anthropogenic carbon uptake in the two runs, the results in 1995 are chosen for comparison with the results of Gruber et al. (2009). The uptake in these three regions is calculated according to Gruber et al. (2009), and the results of Gruber et al. (2009) are obtained from their Fig. 1. As shown in Table 1, in the tropics (18°S–18°N) the results of our two runs are quite consistent with the results of Gruber et al. (2009), with uptake >0.3 Pg C yr^{-1} in 1995. Unlike in the tropical region, there is an obvious difference between the two runs in the southern and northern subtropical regions. From 18°N to 49°N, the uptake obtained in BIO is 0.17 Pg C yr^{-1}, which agrees well with the result of ∼0.18 Pg C yr^{-1} of Gruber et al. (2009) but is ∼1.5 times as large as that of PTB. In this region, the obvious difference in the flux between the two runs and the weak vertical ventilation there lead to that although the Revelle factor in the subtropical North Pacific is larger in BIO than in PTB, the surface anDIC concentration is still higher in BIO than in PTB. From 18°S to 44°S, the uptake in BIO is also much larger than that in PTB. With the smaller Revelle factor in BIO, the larger flux in BIO makes that the surface anDIC concentration is much higher in BIO than in PTB in the subtropical South Pacific. With respect to the almost equal quantities of the uptake in two subtropical regions in PTB, the result of Gruber et al. (2009) showed that the ability of absorbing anthropogenic CO_2 in the southern subtropical region was obviously weaker than that in the northern subtropical region, a result that is in agreement with that of BIO. This implies that, for the difference of the uptake between in the southern and northern subtropical regions in BIO, the distribution of biogeochemical variables other than anDIC is probably a main cause.

Table 1. Total uptake of anthropogenic carbon in three regions in 1995 (Pg C yr^{-1}).

	44°–18°S	18°S–18°N	18°–49°N
Gruber et al. (2009)	∼0.10	∼0.32	∼0.18
BIO	0.15	0.30	0.17
PTB	0.11	0.33	0.11

To determine the main regions of greatest difference between the two runs, the Pacific Ocean is divided into more detailed regions (Table 2). The two runs reveal the largest uptake at 50°–60°S, and another large uptake at 20°S–20°N. Although in the tropics (20°S–20°N) the difference in the total uptake rate between the two runs is only 0.01 Pg C yr^{-1}, the difference is >0.03 Pg C yr^{-1} at each 10° band of latitudes because BIO has two uptake centers in the equatorial region. On the other hand, the difference in the uptake rate between the two runs exhibits a distribution pattern of equatorial symmetry: in the region equatorward of 10°S and 10°N and the region polarward of 40°S and 40°N, the uptake rate is larger in PTB than in BIO but smaller at 10°–40° in both hemispheres. Meanwhile, the absolute difference in the uptake rate between the two runs generally decreases with increasing latitude, whereas the relative difference reaches the largest value of 131% at 20°–30°N. At 20°–30°S, the relative difference is ∼70%. The distribution charac-

Table 2. Total uptake of anthropogenic carbon in the different regions of the Pacific Ocean in the two runs in 1995.

Area	BIO ($\times 10^{-2}$ Pg C yr^{-1})	PTB ($\times 10^{-2}$ Pg C yr^{-1})	BIO-PTB ($\times 10^{-2}$ Pg C yr^{-1})	(BIO-PTB)/PTB (%)
50°–65°N	1.77	2.04	−0.63	−30.9
40°–50°N	3.93	4.18	−0.25	−6.0
30°–40°N	6.11	4.01	2.1	52.4
20°–30°N	4.81	2.08	2.73	131.2
10°–20°N	8.71	5.38	3.33	61.9
0°–10°N	5.66	10.24	−4.58	−44.7
10°S–0°	7.41	11.95	−4.54	−38.0
20°–10°S	11.47	6.75	4.72	69.9
30°–20°S	5.68	3.40	2.28	67.1
40°–30°S	4.63	4.30	0.33	7.7
50°–40°S	6.47	6.56	−0.09	−1.4
60°–50°S	11.32	13.12	−1.8	−13.7
70°–60°S	7.35	8.10	−0.75	−9.3
75°–70°S	0.54	0.51	0.03	5.0

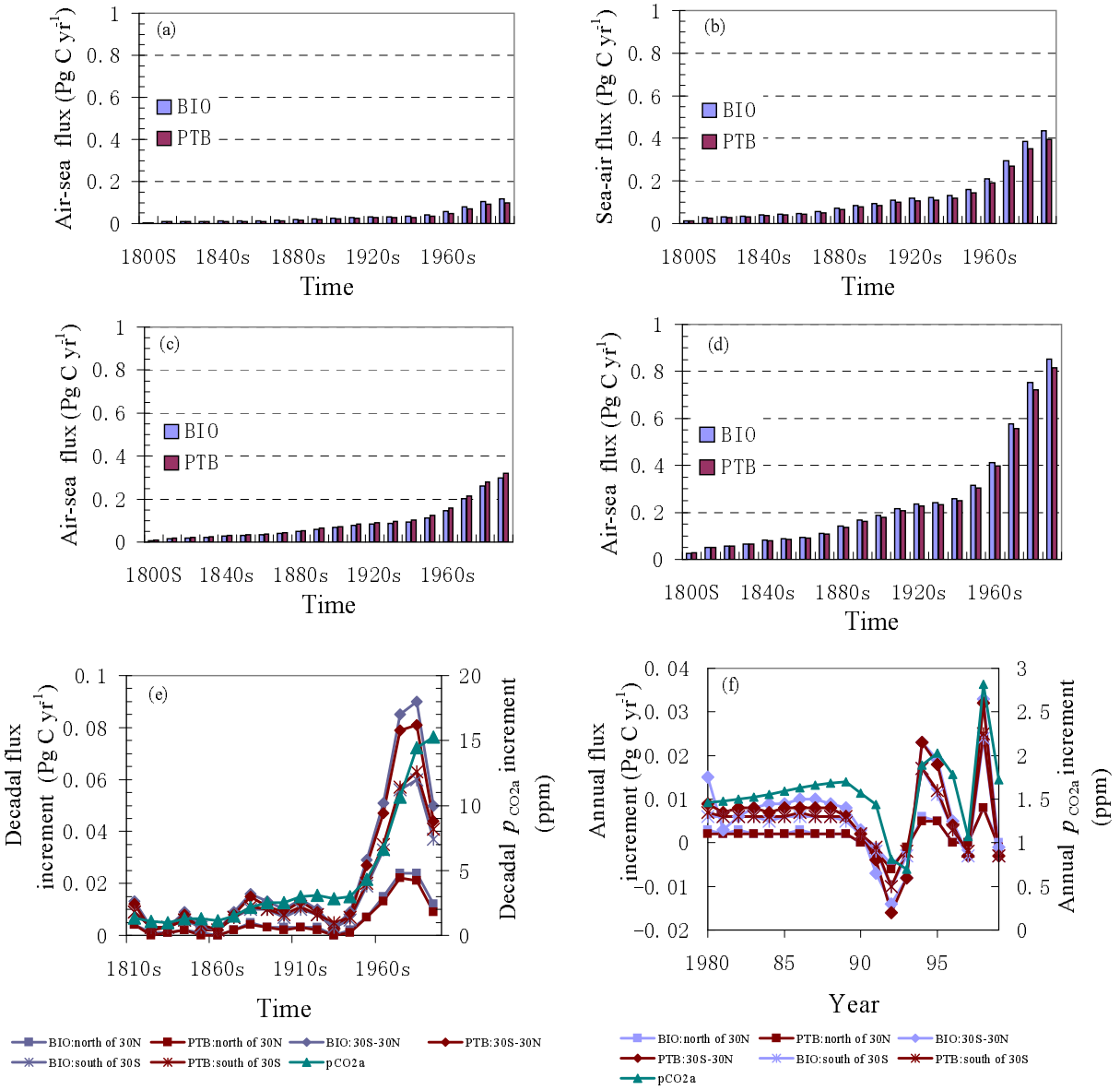

Fig. 8. Decadal mean uptake rate of anthropogenic CO_2 for three regions from the two runs: (a) the northern North Pacific, (b) the Tropical Pacific, (c) the southern South Pacific, and (d) whole Pacific Ocean, (e) decadal flux increment and decadal $p_{CO_{2a}}$ increment, and (f) annual flux increment and annual $p_{CO_{2a}}$ increment.

teristic of the relative difference is broadly consistent with the TA distribution characteristic in BIO: The large relative difference corresponds to the large TA value. This illustrates that the horizontal distribution of TA can affect the simulated results to large extent.

Table 2 shows that the largest difference between the two runs appears to be at the region of 30°S–30°N (tropics). To examine the variation of the difference among the main region and other regions during the time integration, the boundary of 30° is chosen to divide the Pacific Ocean into three regions meridionally. Thereby, the northern North Pacific (north of 30°N) has a surface area of 2.57×10^{13} m^2, the Tropical Pacific has a surface area of 1.06×10^{14} m^2, and the southern South Pacific (south of 30°S) 4.60×10^{13} m^2. As shown in Fig. 8, the largest uptake is located in the Tropical Pacific with the 10-year averaged flux of 0.44 Pg C yr^{-1} in BIO and 0.40 Pg C yr^{-1} in PTB in the 1990s, but the area mean uptake rate in the southern South Pacific is the largest one in the three regions. The air-sea exchange flux of anthropogenic carbon in the whole Pacific Ocean is 0.85 Pg C yr^{-1} and 0.81 Pg C yr^{-1} in the 1990s in BIO and PTB, respectively.

As the integration proceeds, the absolute difference

in the uptake rate between the two runs increases with time in all three regions, whereas the relative difference has small variations. After 1850, in the northern North Pacific, the relative difference varies with 14%–21%, whereas it varies 8%–10% and −6%−−9% in the Tropical Pacific and the southern South Pacific, respectively. In the whole Pacific Ocean, the relative difference is almost constant at 4.5%, which indicates that the difference between the two runs is probably induced by a factor that is nearly constant with the change of anDIC.

Distinct variations in the decadal increment of 10-year mean fluxes between the adjacent decades (Fig. 8e) are seen. The decadal flux (or $p_{CO_{2a}}$) increment in the 1990s in Fig. 8e is the difference in 10-year mean fluxes (or $p_{CO_{2a}}$) between the 1990s and 1980s. The exchange fluxes generally increase with the increase of $p_{CO_{2a}}$, whereas the rate of change in the fluxes certainly decreases when the rate of change in $p_{CO_{2a}}$ decreases. Furthermore, in some decades, although the decadal $p_{CO_{2a}}$ increment increased, the decadal flux increment decreased. For example, compared to the 1970s, $p_{CO_{2a}}$ in the 1980s greatly increased, and correspondingly the flux also greatly increased. However, although the decadal $p_{CO_{2a}}$ increment in the 1990s was larger than that in the 1980s, the decadal flux increment in the 1990s greatly decreased relative to that in the 1980s.

To explain this phenomenon, the flux and atmospheric CO_2 in the 1980s and 1990s are chosen for our analysis of the relation between the flux increment and the $p_{CO_{2a}}$ increment (Fig. 8f). In the 1980s the annual $p_{CO_{2a}}$ increment continuously increased with time, and correspondingly the annual flux increment maintained a consistently positive value, whereas in the1990s when the annual $p_{CO_{2a}}$ increment underwent a great variation, the annual flux increment correspondingly revealed an obvious interannual variation. Annual increment of flux or $p_{CO_{2a}}$ is defined as the difference in annual total flux or annual mean $p_{CO_{2a}}$ between the two adjacent years. When the annual $p_{CO_{2a}}$ increment weakens, the annual total flux increment also weakens and even appears to be negative. In other words, whether the air-sea flux can increase with time depends not only on the increase of $p_{CO_{2a}}$, but more importantly on the rate of change in $p_{CO_{2a}}$. The same conclusion can also be drawn from Eq. (13) of Sarmiento et al. (1995), which indicates that the differential uptake is proportional to the time derivative of atmospheric CO_2 concentrations. In the 1990s, the frequent ENSO events induced the large fluctuation in the annual $p_{CO_{2a}}$ increment because of the large fluctuation of the land and ocean CO_2 fluxes, which led to the great decrease in the rate of change in the air-sea carbon flux, although the 10-year $p_{CO_{2a}}$ increment in the 1990s was larger than that in the 1980s.

4. Conclusions

We employ a Pacific Ocean general circulation model to estimate the uptake and storage of anthropogenic CO_2 in the Pacific Ocean in terms of two different runs with the biogeochemistry (BIO) and perturbation (PTB) approaches.

The distribution of simulated anthropogenic carbon in the Pacific Ocean is consistent with the observation-based estimate in most regions. There is some difference in the surface anDIC concentration between the two runs. This difference seems to be related to the use of globally constant TA and salinity in PTB, which reduces the Revelle factor in the North Pacific and Southern Ocean but increases it in the subtropical South Pacific. Most of the anthropogenic carbon that is mainly absorbed in the eastern equatorial Pacific, the western North Pacific, and the Southern Ocean is stored in the subtropical region of the two hemispheres. The simulated results of BIO and PTB show that, as of 1994, the Pacific Ocean (120°E–70°W) contained 46.2 Pg C and 43.2 Pg C of anthropogenic carbon, respectively. These results agree well with the observation-based estimate of 44.5 Pg C. In addition, in BIO and PTB the North Pacific contained 17.0 Pg C and 15.1 Pg C of anthropogenic carbon with the total uptake of 16.1 Pg C and 14.4 Pg C, respectively, indicating that some anthropogenic carbon was transported into the North Pacific from the South Pacific in these simulations.

Generally both runs yield broadly consistent results of the vertical distributions of anthropogenic CO_2 with the similar patterns and penetration depth, which are also in agreement with the observations. It can be concluded from the comparison with the observation-based estimates that under the forcing of climatological data, the estimates of anthropogenic CO_2 by two approaches are reasonable. Meanwhile, our physical model and biogeochemistry models can be considered reliable.

The air-sea exchange flux of anthropogenic CO_2 in the whole Pacific Ocean is 0.85 Pg C yr^{-1} and 0.81 Pg C yr^{-1} in BIO and PTB in the 1990s, respectively. Although the two runs basically generate the same features of the fluxes, there are some obvious differences between the two runs in the details because of the impacts of total alkalinity. For example, there is only a maximum flux area located south of the equator in the tropics in PTB, whereas BIO has two maximum flux areas, including one south of the equator and the other located at 10°–20°N. For the comparison in each 10°

zonal band, the relative difference in the annual total uptake between the two runs in 1995 is associated with the TA distribution in BIO.

As $p_{CO_{2a}}$ increases with time, the variation of the relative difference in the uptake between the two runs with time is small after 1850, with a nearly constant of 4.5% in the whole Pacific Ocean. Further analysis indicates that in both runs there are considerable variations in the decadal flux increment. The flux increases with the increase of atmospheric p_{CO_2}. In most decades the decadal flux increment increased with increasing $p_{CO_{2a}}$, but in some decades it decreased while the decadal $p_{CO_{2a}}$ increment increased during the same period, especially in the 1990s. The increment of the fluxes is associated with the rate of change in atmospheric p_{CO_2}, so that there were many negative increments of the annual mean flux in the 1990s due to the negative annual increments of atmospheric p_{CO_2}. These negative interannual increments of the fluxes resulted in the small decadal increment in the 1990s, even smaller than in the 1970s.

Acknowledgements. This work was supported by the Research and Development Special Fund for Public Welfare Industry (Meteorology) (Grant No. 2008416022), the National Natural Science Foundation of China (Grant No. 40730106), the National Basic Research Program of China ("973 program", Grant No. 2010CB951802) and the Ocean Public Welfare Scientific Research Project, State Oceanic Administration of the People's Republic of China (Grant No. 200905012-4).

REFERENCES

Anderson, L., and J. Sarmiento, 1995: Global ocean phosphate and oxygen simulations. *Global Biogeochemical Cycles,* **9**, 621–631.

Enting, I. G., T. Wigley, M. Heimann, Eds., 1994: Future emissions and concentration of carbon dioxide: Key ocean/atmosphere/land analysis. CSIRO Division of Atmospheric Research Technical Paper, No. 31, CSIRO, Australia.

Esbensen, S. K., and Y. Kushnir, 1981: The heat budget of the global ocean: An atlas based on estimates from surface marine observations. Tech. Rep. 29, Climatic Research Institute, Oregon State University, 244pp.

Friedlingstein, P., and Coauthors, 2006: Climate-carbon cycle feedback analysis: Results from the C^4MIP model intercomparison. *J. Climate*, **19**, 3337–3353

Gnanadesikan, A., J. P. Dunne, R. M. Key, K. Matsumoto, J. L. Sarmiento, R. D. Slater, and P. S. Swathi, 2004: Oceanic ventilation and biogeochemical cycling: Understanding the physical mechanisms that produce realistic distributions of tracers and productivity. *Global Biogeochemical Cycles*, **18**, doi: 10.1029/2003GB002097.

Gent, P. R., and J. C. McWilliams, 1990: Isopycnal mixing in ocean circulation models. *J. Phys. Oceanogr.*, **20**, 150–155.

Gent, P. R., J. Willebrand, and T. J. McDougall, 1995: Parameterizing eddy-induced tracer transports in ocean circulation models. *J. Phys. Oceanogr.*, **25**, 463–474.

Gloor, M., N. Gruber, J. L. Sarmiento, C. L. Sabine, R.A. Feely, and C. Roedenbeck, 2003: A first estimate of present and pre-industrial air-sea CO_2 fluxes patterns based on ocean interior carbon measurements and models. *Geophys. Res. Lett.*, **30**(1), 1010, doi: 10.1029/2002GL015594.

Gruber, N., and Coauthors, 2009: Oceanic sources, sinks, and transport of atmospheric CO_2. *Global Biogeochemical Cycles,* **23**, GB1005, doi: 1029/2008GB003349.

Keeling, C. D., 1968: Carbon dioxide in surface ocean waters, 4. Global distribution. *J. Geophys. Res.*, **73**, 4543–4553.

Key, R. M., and Coauthors, 2004: A global ocean carbon climatology: Results from Global Data Analysis Project (GLODAP). *Global Biogeochemical Cycles*, **18**, GB4031, doi: 10.1029/2004GB002247.

Lachkar, Z., J. C. Orr, and J.-C. Dutay, 2009: Seasonal and mesoscale variability of oceanic transport of anthropogenic CO_2. *Biogeosciences*, **6**, 2509–2523.

Le Quéré, C., J. C. Orr, P. Monfray, O. Aumont, and G. Madec, 2000: Interannual variability of the oceanic sink of CO2 from 1979 through 1997. Global Biogeochemical Cycles, **14**, 1247–1265.

Liu, H. L., X. H. Zhang, W. Li, Y. Y. Yu, and R. C. Yu, 2004: An eddy-permitting oceanic general circulation model and its preliminary evaluation. *Adv. Atmos. Sci.*, **21**, 675–690.

Matsumoto, K., and Coauthors, 2004: Evaluation of ocean carbon cycle models with observation-based metrics. *Geophys. Res. Lett.*, **31**, doi: 10.1029/2003GL018970.

Mikaloff Fletcher, S. E., and Coauthors, 2006: Inverse estimates of anthropogenic CO_2 uptake, transport, and storage by the ocean. *Global Biogeochemical Cycles*, **20**, GB2002, doi: 10.1029/2005GB002530

Müller, S. A., F. Joos, N. R. Edvards, and T. F. Stocker, 2006: Water mass distribution and ventilation time scales in a cost-efficient, three-dimensional ocean model. *J. Climate*, **19**, 5479–5499.

Murnane, R. J., J. L. Sarmiento, and C. Le Quere, 1999: Spatial distribution of air-sea CO_2 fluxes and the interhemisopheric transport of carbon by the oceans. *Global Biogeochemical Cycles*, **13**, 287–305.

Najjar, R. G., J. L. Sarmiento, , and J. R. Toggweiler, 1992: Downward transport and fate of organic matter in the ocean: simulations with a general circulation model. *Global Biogeochemical Cycles*, **6**, 45–76.

Najjar, R. G., and Coauthors, 2007: Impact of circulation on export production, dissolved organic matter and dissolved oxygen in the ocean: Results from Phase II of the Ocean Carbon-cycle Model Intercomparison

Project (OCMIP-2). *Global Biogeochemical Cycles*, **21**, GB3007, doi: 10.1029/2006GB002857.

Orr, J., and Coauthors, 2001: Estimates of anthropogenic carbon uptake from four 3-D global ocean models. *Global Biogeochemical Cycles*, **15**, 43–60.

Peng, T.-H., 1987: Seasonal variability of carbon dioxide, nutrients and oxygen in the northern North Atlantic surface water: Observations and a model. *Tellus*, **39B**, 439–458.

Roeske, F., 2001: An atlas of surface flues based on the ECMWF re-analysis—A climatological dataset to force global ocean general circulation models. Repor No. 323, Max-Planck-Institut für Meteorologie, Hamburg, 1–31.

Rodgers, K. B., J. L. Sarmiento, O. Aumont, C. Crevoisier, C. B. Montegut, and N. Metzll, 2008: A wintertime uptake window for anthropogenic CO_2 in the North Pacific. *Global Biogeochemical Cycles*, **22**, doi: 10.1029/2006GB002920.

Sabine, C. L., and Coauthors, 2002: Distribution of anthropogenic CO_2 in the Pacific Ocean. *Global Biogeochemical Cycles*, **16**(4), 1083, doi: 10.1029/2001GB001639.

Sabine, C. L., and Coauthors, 2004: The oceanic sink for anthropogenic CO_2. *Science*, **305**(16), 367–371.

Sabine, C. L., R. A. Feely, F. J. Millero, A. G. Dickson, C. Langdon, S. Mecking, and D. Greeley, 2008: Decadal changes in Pacific carbon. *J. Geophys. Res.*, **113**, doi: 10.1029/2007JC004577.

Sarmiento, J. L., J. C. Orr, and U. Siegenthaler, 1992: A perturbation simulation of CO_2uptake in an ocean general circulation mode. *J. Geophys. Res.*, **97**, 3621–3645.

Sarmiento, J. L., C. Le Quéré, and S.W. Pacala, 1995: Limiting future atmospheric carbon dioxide. *Global Biogeochemical Cycles*, **9**, 121–138.

Siegenthaler, U., and F. Joos, 1992: Use a simple model for studying oceanic tracer distributions and the global carbon cycle. *Tellus*, **44B**, 186–207.

Solomon, S., D. H. Qin, M. Manning, M. Marquis, K. Averyt, M. M. B. Tignor, H. L. Jr. Miller, and Z. L.Chen, 2007: *Climate Change 2007: The Physical Science Basis. Contribution of Working Group I to the Fourth Assessment Report of the Intergovernmental Panel on Climate Change*, Cambridge University Press, Cambridge, United Kingdom and New York, NY, USA, 996pp.

Sweeney, C., E. Gloor, A. R. Jacobson, R. M. Key, G. Mckinley, J. L. Sarmietnto, and R.Wannikhof, 2007: Constraining global air-sea gas exchange for CO_2 with recent bomb ^{14}C measurements. *Global Biogeochemical Cycles*, **21**, GB2015, doi: 10,1029/2006GB002784.

Takahashi, T., and Coauthors, 2002: Global sea-air CO_2 flux based on climatological surface ocean pCO_2, and seasonal biological and temperature effects. *Deep Sea Res. II*, **49**, 1601–1622.

Takahashi, T., and Coauthors, 2009: Climatological mean and decadal change in surface ocean pCO_2, and net sea-air CO_2 flux over the global oceans. *Deep-Sea Res. II*, **56**, 554–577.

Wanninkhof, R., 1992: Relationship between wind speed and gas exchange over the ocean. *J. Geophys. Res.*, **97**, 7373–7382.

Xu, Y. F., 1992: The buffer capability of the ocean to increasing CO_2. *Adv. Atmos. Sci.*, **9**, 501–510.

Xu, Y. F., and Y. C. Li, 2009: Estimates of anthropogenic CO_2 uptake in a global ocean model. *Adv. Atmos. Sci.*, **26**(2), 265–274.

Xu, Y. F., Y. W. Watanabe, S. Aoki, and K. Harada, 2000: Simulations of storage of anthropogenic carbon dioxide in the North Pacific using an ocean general circulation model. *Marine Chemistry*, **72**, 221–238.

Xu, Y. F., Y. C. Li, L. Zhao, R. F. Li, and Y. Q. Yu, 2006: A basinwide ocean general circulation model of the Pacific Ocean and its simulation results. *Chinese J. Atmos. Sci.*, **30**(5), 927–938. (in Chinese)

Yamanaka, Y., and E. Tajika, 1996: The role of the vertical fluxes of particulate organic matter and calcite in the oceanic carbon cycle: Studies using an ocean biogeochemical general circulation model. *Global Biogeochemical Cycles*, **10**, 361–382.

Yuan, D. L., and H. L. Liu, 2009: Long-wave dynamics of sea level variations during Indian Ocean Dipole events. *J. Phys. Oceanogr.*, **39**, 1115–1132, doi: 10.1175/2008JPO3900.1.